Cessation of Porous Layer Growth in n-InP Anodised in KOH

Robert P. Lynch,[a,b] Nathan Quill,[a,b] Colm O'Dwyer,[c,d] Monika Dornhege,[e] Harm H. Rotermund [e,f] and D. Noel Buckley [a,b]

[a]*Department of Physics and Energy, University of Limerick, Limerick Ireland*
[b]*Materials and Surface Science Institute, University of Limerick, Limerick Ireland*
[c]*Applied Nanoscience Group, Department of Chemistry, University College Cork, Cork Ireland*
[d]*Micro & Nanoelectronics Centre, Tyndall National Institute, Lee Maltings, Cork, Ireland*
[e] *Surface Imaging Group, Fritz-Haber-Institute of the Max-Planck-Society, Department of Physical Chemistry, Berlin, Germany*
[f] *Surface Reaction Imaging Group, Department of Physics and Atmospheric Science, Dalhousie University, Halifax, Nova Scotia, Canada*

Anodisation of n-InP in KOH results in the formation of porous layers with a finite thickness. The reason for the cessation of porous etching is believed to be the formation of insoluble precipitates within the pores. Electron micrographs of mature porous layers show significant precipitates within the porous structure. An *in-situ* microscopy study of the surface of InP electrode during anodisation reveals the formation of a layer on the surface. This layer emerges from a point on the surface and quickly spreads across it. This is likely to be the spread of precipitation from the saturated solution within the porous structure. However, once a complete porous layer has formed, there should be no significant increase in mass transport requirements through the porous network, leaving the exact mechanism of the precipitation unclear.

INTRODUCTION

Although the formation of porous silicon in HF has long been known,[1-4] the discovery of visible luminescence from porous silicon [5] sparked the surge in research interest in the formation of porosity in other semiconductors. The list of semiconductors that can now be rendered porous electrochemically includes germanium,[6-8] GaP,[9-11] InP,[12-18] GaAs,[19-23] GaN,[24-26] and many others. A range of different pore morphologies can be obtained in these semiconductors by variation of electrolyte type and concentration,[14,27] carrier concentration and substrate orientation,[28,29] as well as the current density or potential used to form the porous structure.[30] A number of theories have been proposed [2-4,31-34] to explain the plethora of pore morphologies that have been observed with various semiconductor/electrolyte combinations but, so far, no one theory has been able to explain all observations.

In our group, we have demonstrated the formation of porous InP in KOH electrolytes in the concentration range 1-17 mol dm^{-3}.[18,35] We have previously shown that pores emerge from pits in the electrode surface[36] and grow and branch along the <111>A crystallographic directions, forming tetrahedral porous domains.[37] However, unlike

porous InP formed in acidic solutions[12-14], in KOH the pore propagation spontaneously halts both in linear-potential-sweep (LPS) and potentiostatic experiments resulting in a rapid decrease in current density. In this paper we will describe the cessation of this pore propagation and examine the possible causes of this cessation.

EXPERIMENTAL

Wafers were monocrystalline, sulfur-doped, n-type indium phosphide (n-InP) grown by the liquid-encapsulated Czochralski (LEC) method and supplied by Sumitomo Electric. They were polished on one side and had a surface orientation of (100) and a carrier concentration of ~5 × 10^{18} cm^{-3}. To fabricate working electrodes, wafers were cleaved into coupons along the natural {011} cleavage planes. Ohmic contact was made by alloying indium to the back of each coupon; the back and the cleaved edges were then isolated from the electrolyte by means of a suitable varnish. The electrode area was typically 0.2 cm^2. Prior to immersion in the electrolyte, the working electrode was immersed in a piranha etchant (3:1:1 H_2SO_4:H_2O_2:H_2O) for 4 minutes and then rinsed with deionized water.

Anodization was carried out in 5 mol dm^{-3} aqueous KOH by linear potential sweep (LPS) experiments at a scan rate of 2 – 2.5 mV s^{-1}. A conventional three-electrode cell configuration was used, employing a platinum counter electrode and a saturated calomel electrode (SCE) to which all potentials are referenced. A potentiostat interfaced to a Personal Computer (PC) was employed for cell parameter control and for data acquisition. All experiments were carried out at room temperature in the absence of light unless otherwise stated.

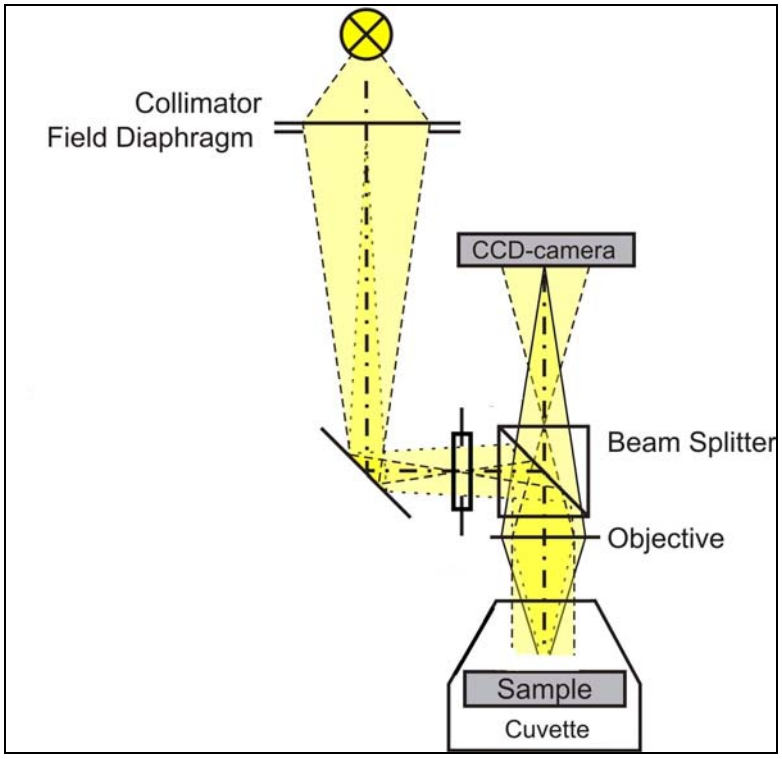

Figure 1. Schematic of optical setup for imaging the electrode surface *in situ* using Köhler illumination at an incident angle of 0°.

In certain experiments low intensity Köhler illumination was used to facilitate *in-situ* microscopy of the electrode surface. We have described the layout of the experiment and the technique in detail elsewhere[38-40]. During potential scans the surface was imaged via optical microscopy with a CCD camera. Great care was taken to synchronize the video sequences and the current versus time curves. A sketch of the optical setup is shown in Fig. 1.

Cleaved {011} cross-sections of the coupons were examined *ex situ* using a Hitachi S-4800 field emission scanning electron microscope (FE SEM) operating at 5 kV. Crystallographic directions were determined by reference to the primary ($0\bar{1}\bar{1}$) and secondary ($0\bar{1}1$) flats of the supplied wafers.

RESULTS AND DISCUSSION

LPS of n-InP in 5 mol dm^{-3} KOH

Anodisation of n-InP samples by linear potential sweep (LPS) was carried out in 5 mol dm^{-3} KOH at a scan rate of 2.5 mV s^{-1}. The resulting linear-sweep voltammogram (LSV) is shown in Fig. 2c. Marked on the LSV are the pitting potential E_{pit}, the position of the first current peak (P_1) and the position of the second current peak (P_2). After E_{pit} the current rapidly increase until it reaches the current of P_1. During this period, isolated porous domains can be observed on SEM cross section (*e.g.* Fig. 2a). After a short decay in current due to the merging of separate porous domains into a complete porous layer[41], the current begins to increase with potential again, at an approximately linear rate. This approximately linear increase in current is due to the thickening of a fully formed porous layer (*e.g.* as shown in Fig. 2b). Eventually, the current peaks again at P_2 and decays rapidly after that. This rapid decay in current is characteristic of passivation of the electrode against further etching. From this point on the porous layer ceases etching. A further increase of the potential will eventually lead to a change in etching mechanism, initially resulting in the undercutting of the porous layer and etching of the perimeter of the sample[38] followed by electropolishing of the remaining electrode surface.

Similar InP porous layers can be formed in acidic electrolytes such as HCl. Such layers typically exhibit crystallographically oriented porous layers which can readily extend over 30 μm into the InP surface[42] and current-line oriented porous layers which can extend over 100 μm into the InP surface[43]. The possible reasons for the cessation of porous layer growth in InP in KOH will be explored in the ensuing sections.

Formation of Precipitates within the Porous Layer

Porous layers which have been grown to the point of cessation are typically observed to have significant deposits within their porous structure. To study the appearance of such deposits within the pores, a series of samples were anodised by LPS to various peak potentials and the resulting porous layers were examined by scanning electron microscopy (SEM). The top left image in Fig. 3 shows an LSV of an InP electrode in 5 mol dm^{-3} KOH. The four points marked A through D on the LSV indicate the upper potentials of LPSs performed on samples under similar conditions. Figures 3a-3d2 show SEM micrographs of samples swept to points A, B, C and D, on the LSV on the top left of the figure. Image (a) shows an SEM micrograph of the sample that had its potential swept to point A (0.34 V). A typical incomplete porous layer is seen with empty “clean”

pores seen throughout. Images (b1) and (b2) show the upper and lower sections, respectively, of a porous layer grown to point B (0.385 V) in the LSV. The upper section is near the electrode surface, and the lower section is near the bulk InP. The pores in the upper section are again typical empty pores. However, in the lower section of the porous layer a small amount of material can be seen as grainy, roughened deposits in the pores in image (b2). Images (c1) and (c2) show the upper and lower sections, respectively, of a porous layer grown to point C (0.42 V). At this point, even the upper section is showing some deposits within the pores, with large lumps seen to be clogging up some of the pores. In the lower section, deposits can now be seen in almost every pore. Finally, images (d1) and (d2) show the upper and lower sections respectively of a porous layer grown to point D (0.5 V). The upper section of the layer is again filled with many lumps which have a diameter roughly equal to the width of the pore. The lower section in this instance is so completely filled with material that it is difficult to distinguish between deposit-filled pores and bulk InP.

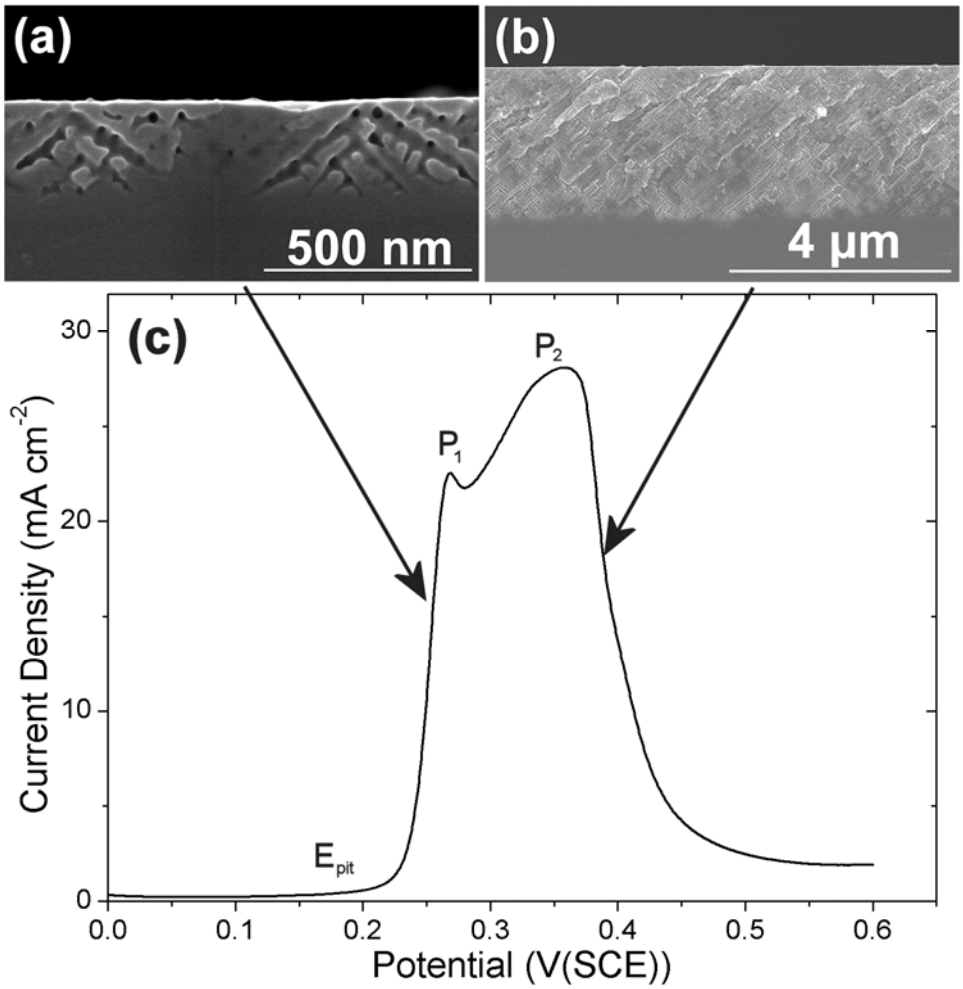

Figure 2. (a) SEM image of two separate porous domains about to merge together, (b) SEM image of a complete porous layer and (c) a LSV of an n-InP sample subjected to an LPS from 0 to 0.6 V at 2.5 mV s^{-1} in 5 mol dm^{-3} KOH. The points marked on the LSV are E_{pit}, the potential at which etch pits appear on the electrode surface, and P_1 and P_2, the first and second current peaks, respectively.

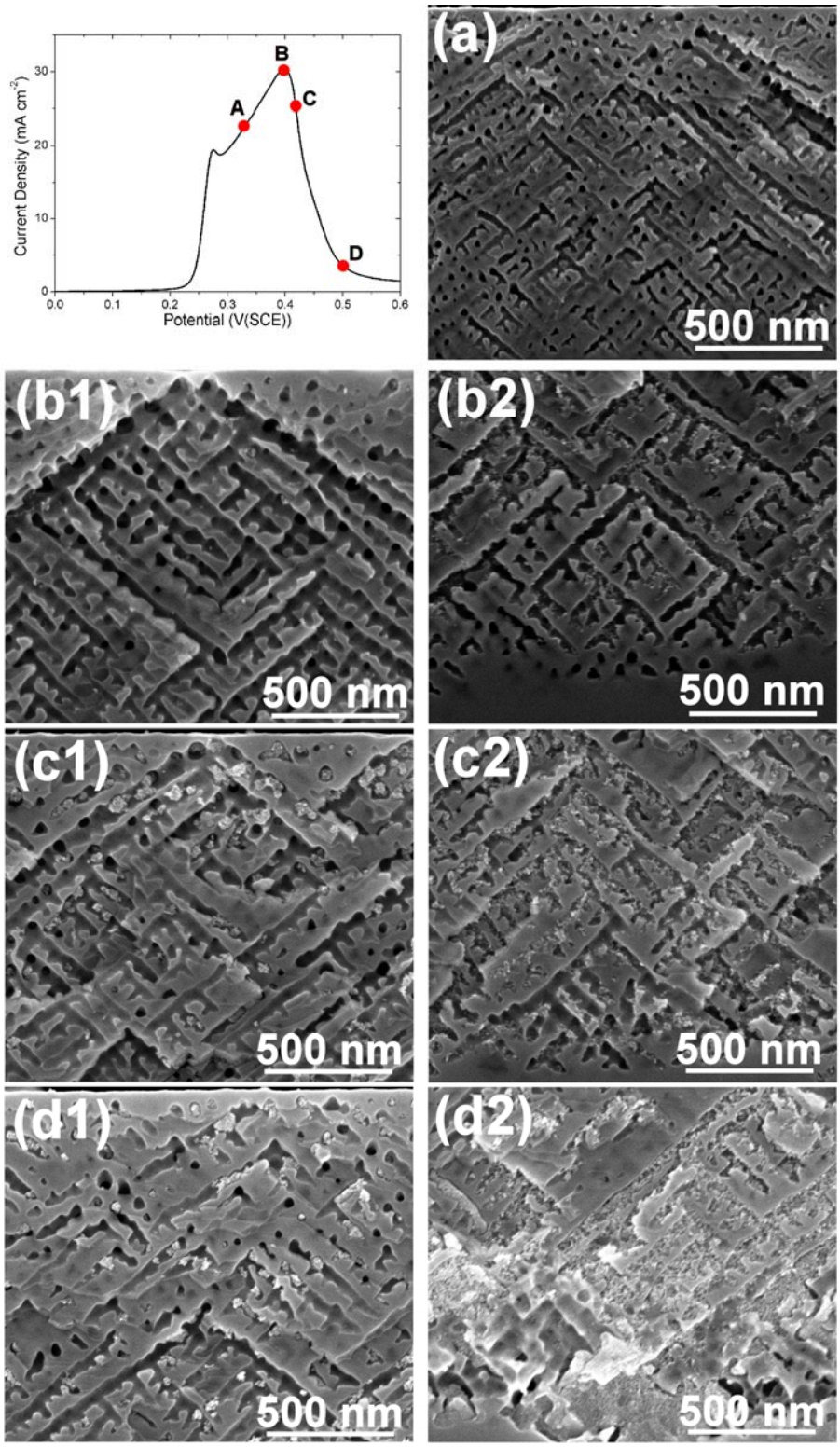

Figure 3. SEM micrographs of InP electrodes which have been subjected to LPSs to potentials indicated on the LSV on the top left of this figure. Images (a), (b), (c) and (d) show porous layer grown to point A (0.33 V), B (0.40 V), C (0.42 V) and D (0.50 V) in the LSV, respectively, where image 1 and 2 of (b), (c) and (d) show the upper and lower section of the respective layers. Image (d) corresponds to a fully grown porous layer.

The micrographs in Fig. 3 show a clear trend. After P_2, the pores begin to fill up with deposits. This indicates a likely correlation between the end of porous layer etching and the appearance of these deposits. In Image (d2) the in filling is so complete as to block the path of the electrolyte through the pores. It seems likely that the formation of this oxide results in the observed decrease in current and the termination of porous layer etching. The oxide is always more abundant near the porous-bulk interface which suggests that its source may be at or near the pore tips. This indicates that the deposits are likely to be composed of at least some of the reaction products of the InP dissolution.

In-situ Observation of Precipitates on the Electrode Surface

Figure 4 shows the process of etching InP, as viewed with a CCD camera, under low intensity Köhler illumination. Several stages can be distinguished during the LPS as discussed previously[38]. During the first 90 s the current increases slowly with increasing applied potential, with no resulting change to the electrode surface (*e.g.* Fig. 4a). Just before 0.2 V, the current begins to increase rapidly and continues to increase until it reaches 44.6 mA cm^{-2}. As the current reaches this first peak the light intensity from the surface reaches a maximum (*e.g.* Fig. 4b) due to the formation of a thin near surface layer of dense InP that is separated from the bulk InP by a continuous porous layer (similar to that shown at A in Fig. 5). Coinciding with the second current peak the electrode surface darkens (*e.g.* Fig. 4c). The current then decreases and simultaneously a bright region appears and grows finger-like into the dark area (as is evident from Figs. 4d and 4e). Once this bright region has spread over the surface the light intensity is relatively unaffected by the anodization process despite the current continuing to increase until the end of the experiment.

The increase in light intensity observed in Fig. 4b has been explained previously by us to be due to constructive interference[38]. Where reflection occurs at a transition from high to low refractive index, the reflected light experiences a phase shift of half a wavelength. Therefore, a very thin layer of InP ($\eta_{InP} \approx 3.7$) will produce two reflected rays that will destructively interfere if it is between electrolyte ($\eta_e \approx 1.4$) and a porous layer that contains electrolyte similar to the bulk electrolyte (*i.e.* $\eta_{pI} < 3.7$). We refer to this situation where the second layer has a higher refractive index than that of the first and third layers as a Type I system. In such a system, if the layer thickness is a quarter of the wavelength of the light constructive interference will occur. Such a condition is met for the thickness of the dense near surface layer.

In a similar manner a very thin layer of InP will produce two reflected rays that will constructively interfere if it is between electrolyte ($\eta_e < \eta_{InP}$) and a porous layer that contains electrolyte of refractive index greater than the that of InP ($\eta_{pII} > 3.7$). We refer to this situation where the refractive index of the third layer is greater than that of the second and the refractive index of the second is greater than that of the first as a Type II system. In such a system, if the layer thickness is a quarter of the wavelength of the light, destructive interference will occur. The required layer thickness, Δt, for constructive and destructive interference maxima can therefore be calculated for both Type I and Type II systems as follows:

Table 1: Conditions for constructive and destructive interference.

Layer Type:	**Type I: $\eta_e < \eta_d > \eta_{pI}$**	**Type II: $\eta_e < \eta_d < \eta_{pII}$**
Destructive Interference:	$\Delta t = \frac{n\lambda_d}{2}$	$\Delta t = \frac{\lambda_d}{4} + \frac{n\lambda_d}{2}$
Constructive Interference:	$\Delta t = \frac{\lambda_d}{4} + \frac{n\lambda_d}{2}$	$\Delta t = \frac{n\lambda_d}{2}$

where n = 0,1,2,3…, λ_d is the wavelength of the light in the medium of the second layer. For In_2O_3 the wavelength of the light is $\lambda_d = \lambda_o/\eta_{ox} \approx 252$ nm (λ_o = 530 nm, In_2O_3 refractive index, $\eta_{ox} \approx 2.1$[44]), and for InP it is $\lambda_d = \lambda_o/\eta_{InP} = 142.6$ nm (InP refractive index, $\eta_d = 3.72$[45]). (The refractive index of the of 5 mol dm^{-3} KOH is $\eta_e = 1.38$.[46]).

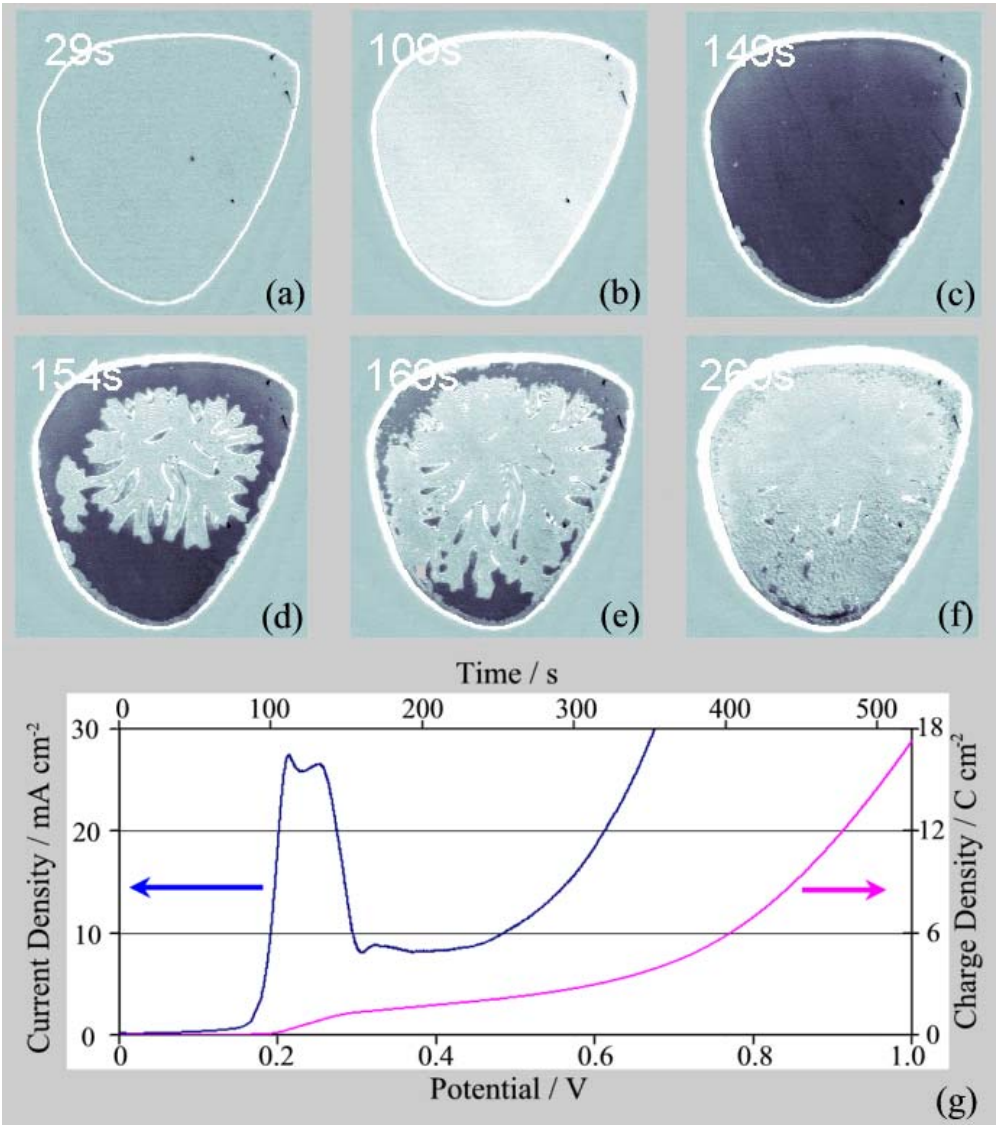

Figure 4. (a-f) *In-situ* microscopy images of the electrode surface during anodisation of InP by LPS. The number of seconds correspond to the points in the voltammogram (LSV) and charge versus potential plot shown in (g). The experiment was carried out under a low intensity of light from 0 to 1 V (SCE) in 5 mol dm^{-3} KOH at 2 mV s^{-1}.

At approximately the same time as the second current-peak (see Fig. 4c), the reflected light from the electrode surface darkens. This outcome could be the result of destructive interference caused by the near-surface layer thinning or thickening or the order of the refractive indexes changing from a Type I to a Type II system. The near-surface layer decreases to 20 nm in some SEM images, accounting for a decrease in light intensity but not for the decrease that is observed. (The light intensity decreases to less than that of the light reflected from the surface at the beginning of the experiment). However, the type of interference could switch from constructive to destructive interference if the order of the refractive indices switched from a Type I to a Type II system, *i.e.* if the refractive index of the material within the pores became greater than that of InP.

As the current decreases after the second current peak, interference fringes appear on and spread out over the electrode surface. These fringes could be caused by the growth of a porous oxide-layer on the surface with constructive or destructive interference occurring depending on the thickness of the porous layer and the order of the refractive indices, *i.e.* whether it is a Type I or Type II system, as shown in Table 1. The propagation of these fringes is impeded by scratches on the surface supporting the conclusion that the fringes are related to phenomena on the electrode surface and not to some sub-surface region of the porous structure. This can be seen in Fig. 5 where the black lines (scratches) divide the fringe regions apart.

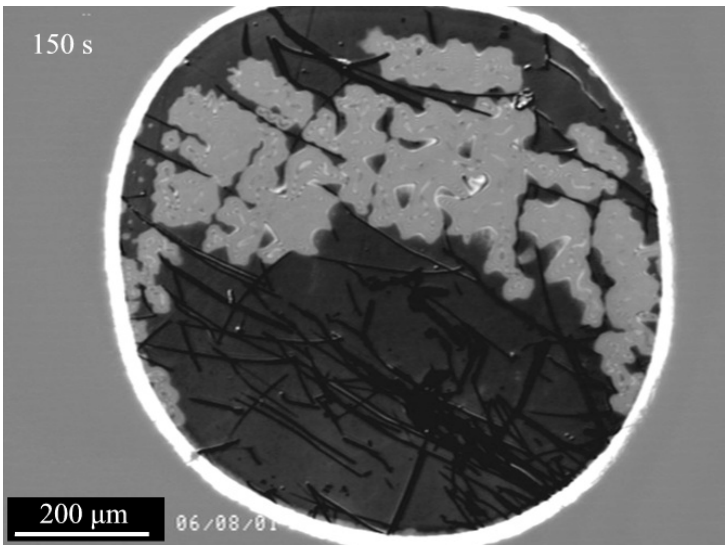

Figure 5: *In-situ* optical microscopy image of the electrode surface at 150 s during an LPS from 0 to 1 V (SCE) in 5 mol dm^{-3} KOH at 2 mV s^{-1}. The surface was scratched prior to etching and these scratches are impeding the progress of the fringe pattern across the electrode surface.

After this decrease in current and the formation of this finger-like pattern of interference fringes, porous layer growth halts and the appearance of the surface changes from being smooth to rough (*e.g.* Fig. 4e to Fig. 4f). This effect starts quickly but then slows down to leave only some small regions that contain interference fringes, but these too eventually disappear. One possibility is that the pits on the electrode surface become blocked, cutting-off the supply of electrolyte and stopping porous layer growth or formation of fresh oxide on the surface. Oxide layers are observed on the surface of fully grown porous layers. In Fig. 6 an oxide layer, approximately 0.72 µm in thickness, can be seen on the surface of the electrode (at C). Energy dispersive X-ray spectroscopy(EDX),

X-ray photo electron spectroscopy (XPS) and electron diffraction studies have shown this oxide to be composed of In_2O_3[47,48]. In_2O_3 is known to be insoluble in all but the most acidic of solutions[49] so it is not surprising that it precipitates during the formation of porous InP in KOH. Assuming a refractive index close to that of In_2O_3, a rough calculation shows that its thickness is sufficient to account for destructive and constructive interference patterns formed on the surface. Furthermore the thickness of the porous layer (at B) is unchanged from the thickness of the porous layer measured by SEM (not shown) for samples anodised by LPS to lower potentials, *i.e.*, the thickness of the porous layer does not increase after the potential of the second peak in current. However, even though the growth of the porous layer stops after this point in the LSV, the current increases. The increase in current has been shown previously to be due to the formation of a trench around the perimeter of the exposed region of the electrolyte[38] (which is observed as a bright outline in *in-situ* microscopy images, *e.g.* Fig. 4f).

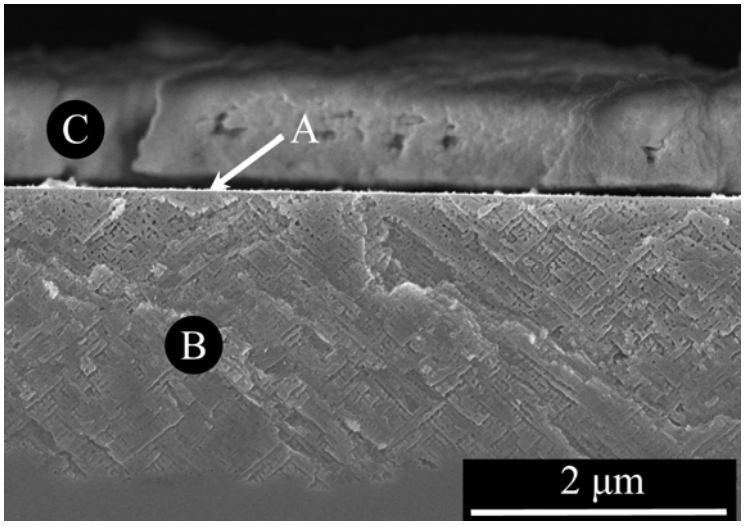

Figure 6: SEM image of porous layer cross-sections (at B) of InP etched in 5 mol dm^{-3} KOH at 2 mV s^{-1} from 0 V to 1 V (SCE) (500 s). The near-surface layer and a thick oxide layer are visible (at A and C, respectively).

Discussion of Diffusion of Ions through the Porous Layer

The observation of oxide deposits within the pores (Fig. 3) appearing after P_2 coupled with the observation of a layer spreading on the surface (Fig. 4) after P_2 would seem to indicate that it is the build up of In oxides in the pores as etching progresses that leads to the cessation of porous layer growth. However, the mechanism by which such an oxide builds up and precipitates is not obvious. As a porous domain emerges from a single pit in the electrode surface, the amount of material that needs to be transported through this surface pit increases rapidly as the domain expands. This is due to each surface pit branching into two pores along the two <111>A directions which point down into the substrate, followed by the subsequent branching of the two new pore tips. All of these new pore tips rely on the lone surface pit as the only pathway to transport etch products out of the porous structure and to transport fresh electrolyte into the porous structure. The surface pit then, is the main mass transport bottleneck during the formation of porous InP. The amount of mass that must be transported through the pit would be expected to increase rapidly as an individual porous domain expands and the number of actively etching pore tips relative to each surface pit increases.

However, once a certain porous layer thickness has been reached (determined by both the final pit density and the rate of pit formation), the individual porous domains merge into a continuous layer. Individual domains can no longer expand laterally, and will only expand deeper into the substrate. Since the pore density and pore width have not been observed to change with porous layer thickness for crystallographically oriented pore etching in KOH, the number of pore tips per porous domain should stay relatively constant after a complete layer has formed. This is because the domain's active etching area can no longer increase by expanding laterally, and the pore tips associated with that domain should always occupy the same area. This indicates that once a complete layer has formed, the rate at which material is being transported through each surface pit has reached a constant value *i.e.* the ratio of the number of pore tips to the number of surface pits is now constant. (Note: in LPS experiments, the current continues to increase in an approximately linear fashion after domain merging has completed, placing a further strain on mass transport processes. However, the same cessation behaviour is observed in potentiostatic experiments in which the current decreases after domain merging has occurred, leading to a decrease in the rate of mass transport through a surface pit.) The expansion and merging of domains is illustrated in Fig. 7 which shows a two dimensional view of the change in active etching area for the porous etching process as individual domains converge to form a continuous porous layer. The red line representing the active etching area is considerably shorter for two merged domains than it is for two isolated domains. The difference in concentration of a particular ion from one side of a surface pit to the other must increase rapidly until the domains have merged. Similarly the change in concentration of this ion between the bulk electrolyte and the pore tips initially increases rapidly as the domains expand. After domain merging, this difference in concentration continues to increase at a much lower rate, due to the thickening of the layer, and in the case of LPS experiments, the approximately linear increase in current density. However, compared to the rapid increase in concentration difference that is observed before domain merging occurred, this increase is much less significant.

If mass transport limitations are the cause of the cessation of porous layer etching, it is much more likely for pore propagation to cease before domain merging has occurred than after. This is what happens in lower carrier concentration electrodes[41]. These electrodes show a single peak in their LSV indicating that the cessation of porous layer etching had begun to occur before a complete porous layer had formed. Higher carrier concentration samples exhibit two peaks in their LSVs and these were shown to be related to domain merging and the cessation of porous layer growth, respectively[41]. In many of these LSVs, the amount of charge passed through the electrode after domain merging is many times the amount of charge passed through the electrode before domain merging. This indicates that domain merging occurred at a shallow layer thickness and that layer thickness increased by a significant amount before the cessation of porous layer etching began. If mass transport difficulties within the porous network result in the build-up and precipitation of oxide within the pores, then this precipitation should occur before the domains have merged and an etch front of constant area has been achieved. Once the domains have merged and a complete layer has formed, one would not expect the concentration of the dissolved oxides within the pores to increase by a significant amount, and the porous layer should be able to thicken continuously without much difficulty.

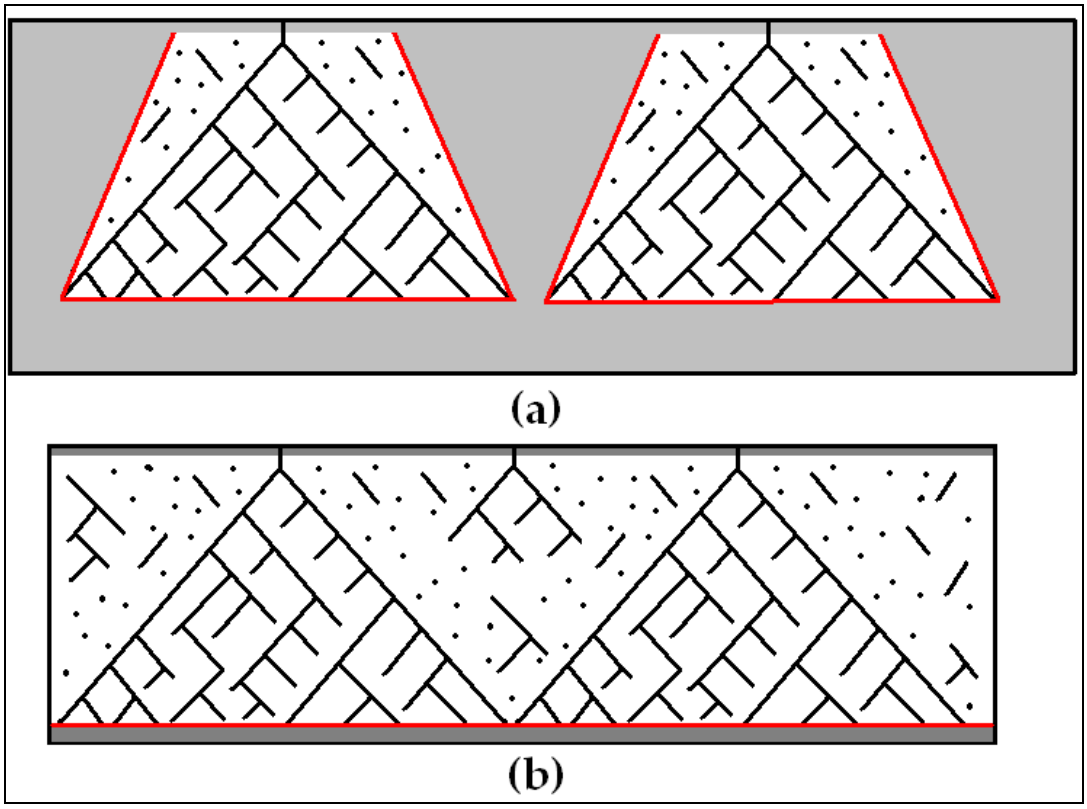

Figure 7. Schematic diagram of the variation in active etching area as (a) individual porous domains expand and (b) as a complete porous layer thickens. The grey areas represent bulk InP. The porous regions have a white background with pores being shown as black lines and dots. The red line indicates the active etching area as seen form this cross section. Clearly the active etching area decreases once a complete layer has formed.

Nevertheless, porous layer etching does cease after a few micrometers, and significant amounts of oxide precipitates are observed in the porous structure. One possible mechanism for the termination of porous layer etching would involve the precipitation of some oxide in just one pore. Some domains will be bigger than others or a region of a domain may expand in a region where it is not competing with other domains (*e.g.* grow a little faster than neighbouring domains). In such situations the concentration of products in a pore may approach saturation rapidly. Where this leads to some oxide precipitates in one of these domains, it may block a number of diffusion pathways for other pores in that domain causing further oxide build up and further precipitation. The precipitation of solids would result in the expansion of the solution within the pores. As the saturated solution spreads throughout the domain and out through the surface pit precipitates will continue to form. These precipitates might restrict diffusion of material through the surface pits of neighbouring domains leading to the saturation of etch products near the pore tips of these domains. Furthermore once etching has ceased in a domain neighbouring domains will expand laterally, rapidly increasing the concentration of products near the pore tips. It follows that once etching ceases in one domain the cessation of etching spreads, explaining what is seen in the *in-situ* optical microscopy experiments shown earlier in Fig. 4. That is, no significant changes occur on the electrode surface between the formation of a complete layer (P_1) and the beginning of the

cessation of porous layer growth (P_2) in these LPS experiments. However, just after P_2, interference patterns start to appear at a small number of points on the surface and begin to spread out over the whole surface. This is most likely the formation of the oxide layer that is seen in SEM images on top of fully grown porous layers (*e.g.* at C in Fig. 6). The fact that this oxide layer emerges from just a small number of points on the electrode surface just after P_2, indicates that it may be precipitation in localized regions of the porous layer that causes the dissolved oxides to precipitate almost simultaneously with the cessation of the thickening of the InP porous layer. That is, the expansion of the material within the pores lead to the transfer of precipitates to the electrode surface which form an oxide layer on the surface. This oxide layer would then block the path of reactants to the pores and trap all of the new products within the porous structure. The concentration of these trapped products within the porous structure would increase quickly, leading to precipitation at almost all of the pore tips. This would explain why oxide is seen in most of the pores near the bottom of a fully etched layer.

The above mechanism relies on the random precipitation of some oxide to commence. This may seem at odds with the relatively consistent layer depths that are observed from experiment to experiment. However, the large number of pores involved (typically $>2\times10^{10}$ cm^{-2} for crystallographically oriented pore layers in KOH) should result in consistent behaviour, even if events are defined by probabilities. For example, surface pits are said to form at defect sites. These defect sites are randomly distributed across the electrode surface, but measurements of pit density are consistent from sample to sample, and the shift in pitting potential from sample to sample is similar to the shift seen in the potential at P_2 from sample to sample. This demonstrates that when such large numbers are involved, even probabilistic events occur consistently.

CONCLUSIONS

Anodisation of InP in KOH results in the formation of a porous layer of finite thickness. This thickness limit is likely due to the low solubility of the products of the etching reaction in alkaline solutions. SEM images of the porous structure reveal that it contains significant oxide deposits within it and is often capped by an oxide layer < 1 μm thick, which is most likely composed of In_2O_3.

Mass transport limitations within the porous layer would seemunlikely to be responsible for the cessation of porous layer growth (*e.g.* through the formation of insoluble oxide precipitates). Significant increases in mass transport through a surface pit should only occur as an individual domain expands laterally in the early stages of porous layer growth and once a complete layer has formed, the rate of mass transport reaches a relatively steady state.

In-situ optical observation of the electrode surface during etching shows what appears to be the spreading of a layer over the whole electrode surface from a single point on the surface. This indicates that it may be oxide precipitation in just a small number of porous domains that causes the cessation of porous etchingvia a domino effect. This domino effect propagates due to the lateral expansion of domains that neighbor domains that have ceased etching and the restriction of diffusion through the surface pits due to the formation of a surface oxide layer. Both of these occurrences lead to the saturation of products near the pore tips and therefore the ceasing of etching in domains that neighbor domains that have ceased etching; *i.e.* the spreading of this oxide layer eventually blocks the surface pits of all domains leading to increased mass transport difficulties in those

domains and the formation of precipitates initially near the pore tips (where the concentration of products is greatest) and then along the pores and over the electrode surface.

ACKNOWLEDGEMENTS

Two of the authors, R.P. Lynch and N. Quill, would like to thank the Irish Research Council for Science Engineering and Technology for postgraduate scholarships to perform this research.

REFERENCES

1. A. Uhlir, *Bell Syst. Tech. J.*, **35**, 333 (1956).
2. M. I. J. Beale, J. D. Benjamin, M. J. Uren, N. G. Chew and A. G. Cullis, *J. Cryst. Growth*, **73**, 622 (1985).
3. R. L. Smith and S. D. Collins, *J. Appl. Phys.*, **71**, R1 (1992).
4. X. G. Zhang, *J. Electrochem. Soc.*, **151**, C69 (2004).
5. L. T. Canham, *Appl. Phys. Lett.*, **57**, 1046 (1990).
6. S. Miyazawa, K. Sakamoto, K. Shiba and M. Hirose, *Thin Solid Films*, **255**, 99 (1995).
7. M. Sendova-Vassileva, N. Tzenov, D. Dimova-Malinovska, M. Rosenbauer, M. Stutzmann and K. V. Josepovits, *Thin Solid Films*, **255**, 282 (1995).
8. S. Bayliss, Q. Zhang and P. Harris, *Appl. Surf. Sci.*, **102**, 390 (1996).
9. B. H. Erne, D. Vanmaekelbergh and J. J. Kelly, *J. Electrochem. Soc.*, **143**, 305 (1996).
10. P. Schmuki, D. J. Lockwood, H. J. LabbeÂ´ and J. W. Fraser, *Appl. Phys. Lett.*, **69**, 1620 (1996).
11. J. Wloka, K. Mueller and P. Schmuki, *Electrochem. Solid-State Lett.*, **8**, B72 (2005).
12. A. Hamamatsu, C. Kaneshiro, H. Fujikura and H. Hasegawa, *J. Electroanal. Chem.*, **473**, 223 (1999).
13. T. Takizawa, S. Arai and M. Nakahara, *Jpn. J. Appl. Phys.*, **33**, L643 (1994).
14. P. Schmuki, L. Santinacci, T. Djenizian and D. J. Lockwood, *Phys. Stat. Sol., A*, **182**, 51 (2000).
15. Z. Weng, A. Liu, Y. Sang, J. Zhang, Z. Hu, Y. Liu and W. Liu, *J. Porous Mater.*, **16**, 707 (2009).
16. Z. Weng, W. Zhang, C. Wu, H. Cai, C. Li, Z. Wang, Z. Song and A. Liu, *Appl. Surf. Sci.*, **256**, 2052 (2010).
17. A. M. Goncalves, L. Santinacci, A. Eb, I. Gerard, C. Mathieu and A. Etcheberry, *Electrochem. Solid-State Lett.*, **10**, D35 (2007).
18. C. O'Dwyer, D. N. Buckley, D. Sutton and S. B. Newcomb, *J. Electrochem. Soc.*, **153**, G1039 (2006).
19. G. Oskam, A. Natarajan, P. C. Searson and F. M. Ross, *Appl. Surf. Sci.*, **119**, 160 (1997).
20. M. M. Faktor, D. G. Fiddyment and M. R. Taylor, *J. Electrochem. Soc.*, **122**, 1566 (1975).
21. P. Schmuki, J. Fraser, C. M. Vitus, M. J. Graham and H. S. Isaacs, *J. Electrochem. Soc.*, **143**, 3316 (1996).

22. I. M. Tiginyanu, V. V. Ursaki, E. Monaico, E. Foca and H. Foll, *Electrochem. Solid-State Lett.*, **10**, D127 (2007).
23. A. M. Gonçalves, L. Santinacci, A. Eb, C. David, C. Mathieu, M. Herlem and A. Etcheberry, *Phys. Stat. Sol., A*, **204**, 1286 (2007).
24. D. J. Diaz, T. L. Williamson, I. Adesida and P. W. Bohn, *J. Vac. Sci. Technol., B*, **20**, 2375 (2002).
25. A. P. Vajpeyi, S. Tripathy, S. J. Chua and E. A. Fitzgerald, *Physica E*, **28**, 141 (2005).
26. F. K. Yam, Z. Hassan, L. S. Chuah and Y. P. Ali, *Appl. Surf. Sci.*, **253**, 7429 (2007).
27. N. Quill, R. P. Lynch, C. O'Dwyer and D. N. Buckley, *Abstracts of Joint 222nd Electrochemical Society Meeting and Fall Meeting of the Electrochemical Society of Japan, Symposium D7: Pits and Pores 5: A Symposium in Honor of David Lockwood,* Honolulu, Hawaii, USA, 7-12 October, abstract 2420 (2012).
28. N. Quill, C. O'Dwyer, R. Lynch and D. N. Buckley, *ECS Trans.*, **19**, 295 (2009).
29. S. Ronnebeck, J. Carstensen, S. Ottow and H. Foll, *Electrochem. Solid-State Lett.*, **2**, 126 (1999).
30. S. Langa, I. M. Tiginyanu, J. Carstensen, M. Christophersen and H. Foll, *Electrochem. Solid-State Lett.*, **3**, 514 (2000).
31. T. Unagami, *J. Electrochem. Soc.*, **127**, 476 (1980).
32. V. Lehmann and H. Foll, *J. Electrochem. Soc.*, **137**, 653 (1990).
33. V. Lehmann, *J. Electrochem. Soc.*, **140**, 2836 (1993).
34. J. Cartensen, M. Christophersen and H. Foll, *Mat. Sci. Eng., B*, **69-70**, 23 (2000).
35. R. P. Lynch, C. O'Dwyer, D. N. Buckley, D. Sutton and S. Newcomb, *ECS Trans.*, **2**, 131 (2006).
36. C. O'Dwyer, D. N. Buckley, D. Sutton, M. Serantoni and S. B. Newcomb, *J. Electrochem. Soc.*, **154**, H78 (2007).
37. R. P. Lynch, C. O'Dwyer, D. Sutton, S. B. Newcomb and D. N. Buckley, *ECS Trans.*, **6**, 355 (2007).
38 R. P. Lynch, M. Dornhege, P. S. Bodega, H. H. Rotermund and D. N. Buckley, *ECS Trans.*, **6**, 331 (2007).
39 M. Dornhege, C. Punckt, J. L. Hudson and H. H. Rotermund, *J. Electrochem. Soc.*, **154**, C24 (2007).
40. C. Punckt, M. Bölscher, H. H. Rotermund, A. S. Mikhailov, L. Organ, N. Budiansky, J. R. Scully and J. L. Hudson, *Science*, **305**, 1133 (2004).
41. N. Quill, C. O'Dwyer, R. Lynch and D. N. Buckley, *ECS Trans.*, **19**, 295 (2009).
42. E. Spiecker, M. Rudel, W. Jäger, M. Leisner and H. Föll, *Phys. Stat. Sol., A*, **202**, 2843 (2005).
43. L. Santinacci, A. M. Goncalves and A. Etcheberry, *ECS Trans.*, **6**, 323 (2007).
44. K.N. Rao, and S. Kashyap, *Surf. Rev. and Lett.* **13**, 221 (2006)
45. D.E. Aspnes and A.A. Studna, *Phys. Rev. B* **27**, 985 (1983)
46. CRC Handbook of Chemistry and Physics 86th ed.: *Physical Constants of Inorganic Compounds,* p. 4-65, D. R. Lide, Editor-in-Chief, CRC Press, New York (2005).
47. N. Quill, *Formation of Nanoporous InP in KOH and KCl: Electrochemistry and Electron Microscopy*, PhD Thesis, University of Limerick, Limerick (2012).
48. C. O'Dwyer, *Anodic Formation and Characterisation of Porous InP in KOH Electrolytes*, PhD Thesis, University of Limerick, Limerick (2003).

49. P. J. Durrant and B. Durrant, *Introduction to advanced inorganic chemistry*, p. 586, Wiley, New York (1970).